MODELING OF SOOTBLOWER JETS AND THE IMPACT ON DEPOSIT REMOVAL IN INDUSTRIAL BOILERS

Markus Bussmann[a]*, Babak Emami[b,c], Danny Tandra[b,d], Wei Yik Lee[a], Ameya Pophali[b,d], Honghi Tran[b]

[a]University of Toronto
Department of Mechanical and Industrial Engineering
Toronto, ON Canada

[b]University of Toronto
Department of Chemical Engineering and Applied Chemistry
Toronto, ON Canada

[c]now with Clyde Bergemann Atlanta, Atlanta, GA, USA

[c]now with Altair Engineering, Mountain View, CA, USA

* corresponding author:

ABSTRACT

Fireside deposit accumulation can be a significant concern in industrial boilers that burn poor quality fuel. Fouling is then commonly controlled by sootblowers, that blast deposits with high pressure supersonic steam or air jets. However, sootblowing is expensive, which motivates efforts to fundamentally understand how sootblower jets behave, and how they interact with heat exchanger geometries and fireside deposits, to guide efforts to improve and optimize sootblower use. Here we first report on the development of a CFD model to predict the flow behaviour of sootblower jets, work that began with the customization of a research code, but has more recently led to the use of the commercial CFD software Fluent, which makes the model more accessible to the wider engineering community. The CFD model has been used to predict sootblower jet pressure and velocity for realistic off-design sootblower jets, as are encountered in practice when the supply pressure to the sootblower does not match the nozzle design pressure. These off-design jets are less efficient, and the way that they interact with heat exchanger configurations and deposits is more complicated than for so-called fully expanded (or ideal) jets. CFD model results are also compared to experimental data that we have obtained for jet flow within model tube bank geometries representative of the superheater and generating bank of an industrial boiler. The results quantify the deposit removal effectiveness of sootblower jets in the different geometries: the centerline rate of decay of so-called peak impact pressure as a function of the relative position of the sootblower nozzle and tube geometry; the strength of the secondary jets that form when a sootblower jet deflects off of a tube; and the force imposed on various tube positions in the different configurations.

KEYWORDS: *sootblowing, deposits, fouling, CFD, supersonic*

1 INTRODUCTION

Fireside deposit accumulation is a significant concern in industrial boilers that burn poor quality fuel, as typically characterized by the ash content. Fouling reduces the thermal efficiency of a boiler, and in severe cases can lead to boiler plugging and unscheduled shutdowns. Both the extent of fouling, and deposit properties, are a function of fuel properties and boiler operating conditions; fouling is much more problematic in, for example, kraft recovery boilers and municipal waste incinerators than in power boilers that burn relatively clean fossil fuels. Nevertheless, with the increasing trend to fuel switching, or the use of fuels for which a boiler was not originally designed, and increasingly to burning waste materials rather than sending them to landfill, boiler fouling is a concern for many boiler operators.

Sootblowers are commonly used to remove fireside deposits from heat transfer surfaces in industrial boilers. Sootblowers utilize boiler steam to generate an opposed pair of supersonic jets that are directed onto deposits; the efficacy of sootblowing is directly related to the jet strength (or force) exerted on deposits during blowing. The required frequency of sootblowing depends on the extent of fouling in a particular boiler: in relatively clean power boilers, sootblowers may be used only occasionally to manage fouling in critical heat exchanger sections; in boilers that burn more challenging fuels, sootblowers may be installed throughout the boiler and operated continuously on a cycle. In those cases, sootblowers can consume a signification fraction (up to 10%) of the steam generated by the boiler, and so represent a significant expense. This motivates research into optimizing sootblowing: maximizing deposit removal and minimizing steam usage.

Over many years, research at the University of Toronto has examined many aspects of sootblower operation; a review of this research, focused largely on experimental work, was presented at the 2010 *Impacts of Fuel Quality* conference held in Saariselkä, Finland [1]. In the current paper we present a more detailed overview of the accompanying research into the development and application of a computational fluid dynamics (CFD) model of a supersonic steam jet, that we have used both to corrobate experimental measurements of sootblower jets, and to provide detailed information (on variations in pressure, velocity, density and Mach number) that cannot be readily measured. In what follows, we present a brief introduction to the physics of sootblower jets, an overview of model developments including the results of various validation tests of our model, and finally sample results of recent calculations of sootblower jet interaction with geometries characteristic of typical heat exchanger sections.

2 BACKGROUND AND MODEL DEVELOPMENT

A sootblower consists of a long lance tube to which high pressure steam is supplied; the end of the lance is capped by a pair of opposed converging-diverging nozzles that can accelerate a flow past Mach 1; such flows are common only in aerospace applications. The number of installed sootblowers will vary with the type and size of boiler, but they all operate by periodically traversing into and out of a heat exchanger section, all the while rotating slowly, as pictured in Figure 1 (left). Unlike subsonic flows, that move at

less than the speed of sound and so react to upstream flow conditions, a supersonic flow is unaware of upstream conditions. Converging-diverging nozzles are characterized by the relative diameters of the throat and exit; isentropic gas dynamics relations then indicate that the pressure at the exit of the nozzle is strictly a function of the supply (or lance) pressure and nozzle geometry. As a result, there is only one supply pressure, the so-called "design pressure", that will yield a steam jet that exits the nozzle at the ambient pressure; that jet is referred to as "fully-expanded". Any other supply pressure will yield a jet that is "off-design", and the exit pressure will not match the ambient pressure. When the supply pressure is greater than the design pressure, the jet pressure at the nozzle exit will be greater than the ambient pressure, and the jet is then characterized as "under-expanded"; conversely, a supply pressure less than the design pressure yields an "over-expanded" jet.

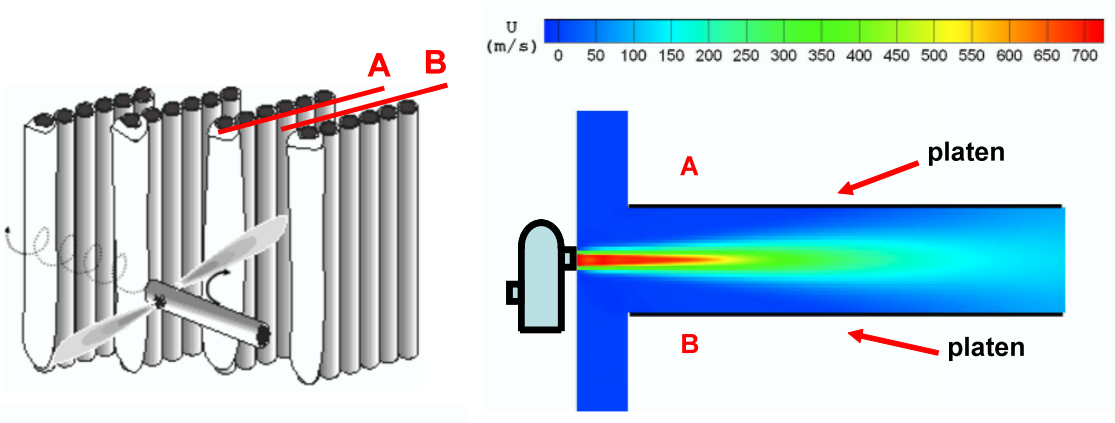

Figure 1. Schematic view of a sootblower jet between superheater platens (left); an axial velocity contour from a simulation of a fully-expanded jet between platens (right).

A fully-expanded jet is characterized by a "supersonic core" within which the flow properties remain almost unchanged from those at the nozzle exit; referring to Figure 1 (right), the core is the red region that extends on the order of 10 nozzle diameters downstream of the nozzle exit. Figure 1 (right) illustrates axial velocity, but pressure and Mach number are also constant within the core, which only ends when the entrained fluid from around the jet eventually reaches the jet centerline. Note that Figure 1 (right) illustrates a very focused jet; this is characteristic of supersonic jets, which spread at a much lower rate than subsonic jets.

At any supply pressure other than the design pressure for a given nozzle, the resulting supersonic jet will be "off-design" because the jet pressure at the nozzle exit will be lower (over-expanded) or higher (under-expanded) than the ambient boiler pressure. Unlike a fully-expanded jet, off-design jets are characterized by a multi-cell shock structure downstream of the nozzle exit that consists of shock and expansion waves, that form as the jet adapts to the ambient pressure. As a result, the centerline pressure along an off-design jet fluctuates above and below the ambient pressure, and due to the waves, such a jet is less efficient than a fully-expanded one.

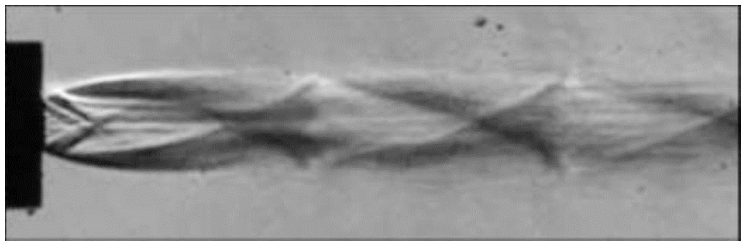

Figure 2. Schlieren image of an under-expanded supersonic jet exiting a nozzle at left. The exit Mach number is 2.53; the pressure ratio $p_e / p_\infty = 3.12$. The lines within the jet correspond to shock and expansion waves as the jet adapts to the ambient pressure.

Much of our CFD model development [2,3] since the mid-1990s utilized the CFDLib research code developed at the Los Alamos National Laboratory, and focused on adapting the standard k-ε turbulence model to turbulent supersonic jet flow, as the code as received (version 3.02) yielded poor predictions even of relatively simple fully-expanded high speed jets; in particular, the code with the standard k-ε model underpredicted various experimentally measured jet core lengths. Tandra [2,4] incorporated the turbulence production model of Heinz [5] to account for structural compressibility effects (related to changes of the structure of velocity fields), and the Durbin realizable model [6] to correct for the overprediction of the growth rate of turbulent kinetic energy in the stagnation zone of an impinging flow. We dubbed this the Sootblower Jet Turbulence (SJT) model, and the improved code CFDLib-SJT.

This model was validated against a wide range of experimental data related to fully-expanded free jets and jets impinging on solid surfaces. Figure 3, for example, illustrates

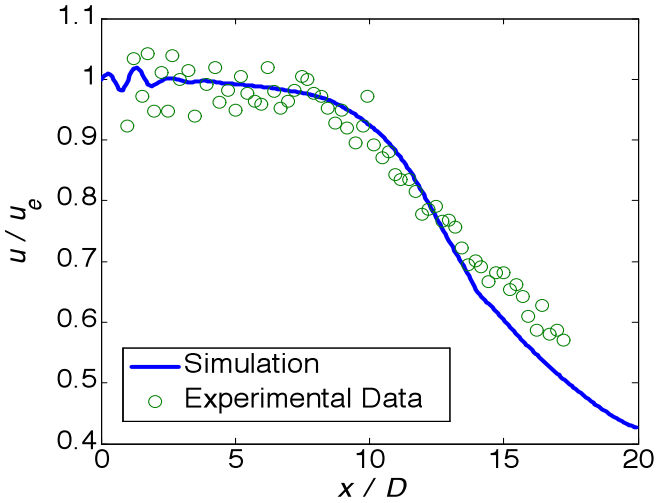

Figure 3. Distribution of the axial velocity along the centerline of a free supersonic jet: comparison of CFDLib-SJT simulation results with the experimental data of Panda and Seasholtz [7]. u_e and D represent the nozzle exit velocity and diameter, respectively.

the axial velocity, u, versus the axial distance from the nozzle exit, x, along the centerline of a fully-expanded jet, compared to the experimental data of Panda and Seasholtz [7]. Notice that the measured velocities fluctuate slightly near the nozzle, as an exactly fully-expanded jet is very difficult to achieve. The corresponding fluctuations in the predicted axial velocity are due to a slight difference between the imposed exit and ambient pressures, the result of truncation errors when calculating the nozzle exit conditions. Nevertheless, the simulation predicts the measurements reasonably well, and the plot illustrates the typical characteristics of a fully-expanded jet: a relatively constant flow for a distance of about 10 nozzle diameters downstream of the nozzle exit (this is the core of the jet), followed by a region in which the velocity decays as the entrained fluid finally reaches the jet centerline.

Figures 4 and 5 illustrate two other validation tests, this time for impinging jets. Figure 4 illustrates the impingement of a subsonic (Mach 0.6, exit velocity 189 m/s) jet onto a hemisphere. The nozzle exit diameter D = 13 mm; the nozzle was mounted 1.96D above the hemisphere surface. The predicted surface pressure distribution agrees very well with the measured data.

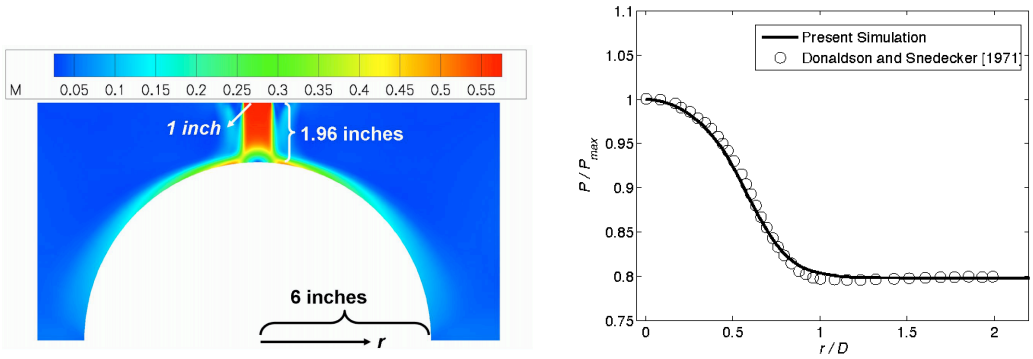

Figure 4. Mach number contours of the impingement of a subsonic (Mach 0.6) jet onto a hemisphere, and the predicted surface pressure distribution versus the experimental data of Donaldson and Snedeker [8].

Figure 5 (left) illustrates the predicted Mach number contours of the fully-expanded supersonic air jet of Carling and Hunt [9], impinging normally on a flat plate. The nozzle exit is half the nozzle diameter D = 23 mm above the plate; the jet has a nozzle exit Mach number of 2.77 (exit velocity of 597 m/s). Figure 5 (right) shows the pressure distribution on the plate surface: the pressure is very high close to the jet centerline, due to the formation of a normal shock wave between the jet and the plate. Away from the centerline, an axisymmetric wall jet forms, consisting of a series of shock and expansion waves (between $r = D$ and $r = 3D$), as evidenced by the pressure fluctuations, through which the pressure drops to the ambient value. The agreement between simulation and experiment is good, especially close to the jet centerline, but even in the wall jet.

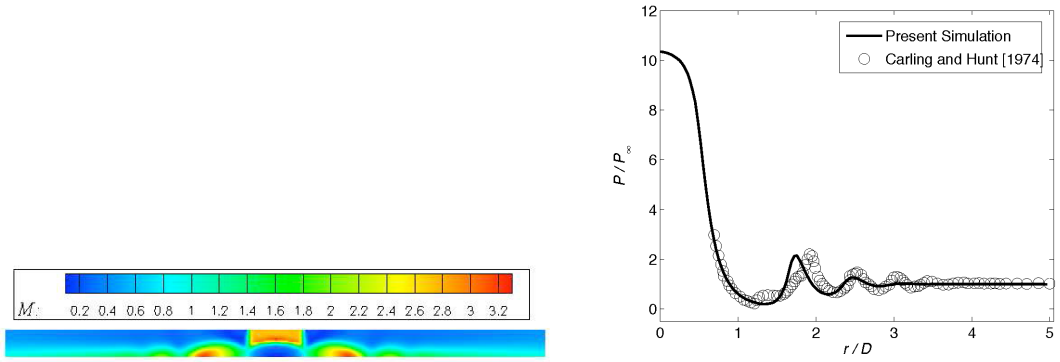

Figure 5. Mach number contours of the impingement of a supersonic (Mach 2.77) jet onto a flat plate, and the predicted far field surface pressure distribution versus the experimental data of Carling and Hunt [9].

The discussion so far has focused on fully-expanded jets, yet in practice, every jet is at least somewhat off-design, as it is impossible to supply a sootblower with pressure at exactly the design pressure. Accurate simulation of such jets required further corrections to the k-ε model, to capture the complex interaction of turbulence and the shock-cell structure that characterizes these jets. By imposing Thivet's realizability constraint on the turbulent eddy viscosity [10], and taking into account shock unsteadiness effects via the correction of Sinha [11], a further-improved turbulence model was developed [3,12], that we dubbed the SJT-shock model.

CFDLib with this latest k-ε turbulence model greatly improved the predictions of off-design jets. Figure 6 (left) presents predictions of centerline pressure versus axial distance from the nozzle exit for the Mach 2.0 under-expanded jet (the pressure ratio p_e / p_∞ = 1.45) of Norum and Seiner [13], using both the SJT and SJT-shock models; Figure 6 (right) presents the corresponding predictions for pressure measured 1/4 nozzle diameter off the centerline. These results are very different from those of Figure 3, in that the pressure even within the core of the jet oscillates strongly as the flow compresses and expands, as it adjusts to the ambient pressure via the shock-cell structure illustrated in Figure 2; the fluctuations die out only many nozzle diameters downstream of the nozzle exit. This can be better seen in Figure 7, which presents the Mach number contours calculated by the SJT-shock model. Returning to Figure 6, notice that the SJT model predicts the positions of the first few waves correctly, but dramatically under-predicts the amplitudes of the waves, which decay much more rapidly than they should. The SJT-shock model, on the other hand, yields a much better agreement with the experimental data, by limiting the rate of dissipation of the jet.

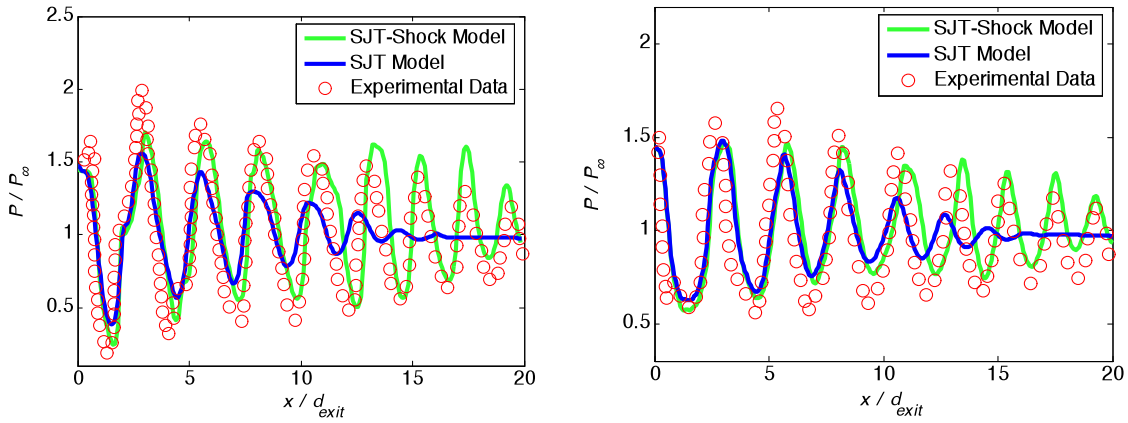

Figure 6. Normalized pressure along the centerline (left) and $0.25d_{exit}$ off the centerline (right), for the off-design jet of Norum and Seiner [13]. P_∞ represents the ambient pressure.

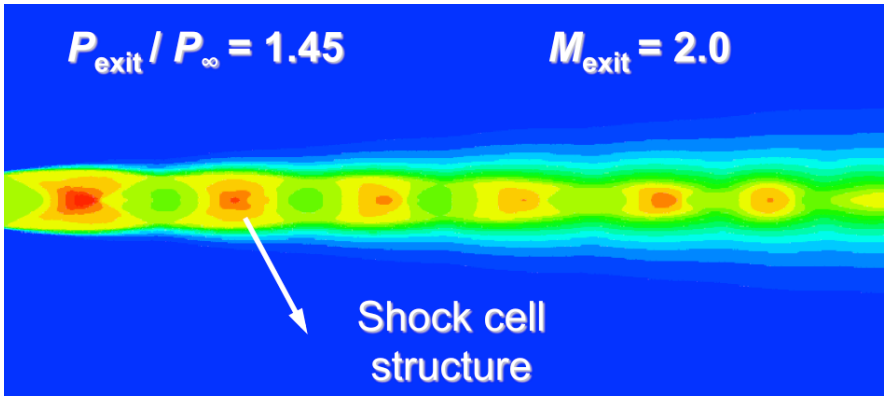

Figure 7. Mach number contours for the off-design jet of Norum and Seiner [13]; red indicates regions of highest Mach number; green regions of lower Mach number.

Finally, we have recently incorporated a subset of the aforementioned turbulence model corrections into the commercial CFD software ANSYS Fluent, via their User Defined Function (UDF) tool and the C++ programming language. ANSYS Fluent is much more versatile than CFDLib from a meshing perspective, and much more user-friendly, and so offers the possibility of examining sootblower jet flow in much more complex geometries.

Most importantly, we installed Heinz's [5] correction for structural compressibility effects, the most important component of the SJT model. (We also disabled the pressure dilatation correlation of Sarkar [14] that is implemented by default in Fluent, that we have found unhelpful for the simulations we run.) On the other hand, we have so far been unable to incorporate the corrections for off-design jets, as the UDF interface does not offer the required code access to make this possible. As a result our Fluent predictions of

off-design free jets are not as accurate as those of CFDLib SJT-shock, but we nevertheless have used this implementation of Fluent to investigate jet/tube interaction, applying it to situations where the distance between the nozzle and the first tube is within a couple of shock cells, beyond which the flows become much more complicated.

3 RESULTS AND DISCUSSION

We now present sample Fluent simulation results of sootblower jet flow interacting with characteristic superheater and generating bank heat geometries, and a comparison of those results with the schlieren images of corresponding flows obtained by Pophali [15].

The schlieren images are of lab-scale (1/4-scale) experiments of supersonic air jet flow onto tube geometries characteristic of kraft recovery boilers. The air was supplied at 2.14 MPa gauge (310 psig) to a converging-diverging nozzle, resulting in a slightly under-expanded primary jet exiting the nozzle at a Mach number of 2.5. All of the results presented here are of a jet impacting normal to a tube geometry, where the distance between the primary jet centerline and the centerline of a row of tubes is defined as the offset ε and non-dimensionalized by the tube outer radius R. The jet that deflects off a first tube is referred to as a secondary jet.

3.1 Sootblower jet flow onto a tube platen

Figure 8 illustrates schlieren images of a jet impacting a row of tubes, representative of the geometry of tube platens in a typical superheater, and corresponding simulation results of jet impingement onto a single tube. The results on the left are for an offset $\varepsilon/R = 0.2$, which is closer to head-on impingement and yields weaker secondary jets that deflect at a larger angle. Note that the schlieren image contains only a single secondary jet, as the flow beneath the tube is obstructed by the tube stand that appears in the lower left corner of the image. The results on the right are for an offset of $\varepsilon/R = 0.6$; the secondary jet in this case is stronger and remains supersonic for a greater distance downstream of the initial impingement. The simulation results clearly capture the gross physics of the flow: the shock and expansion waves in both the primary and secondary jets, as suggested by the corresponding flow characteristics identified by the labels A, B and C, and the simulations yield a reasonable estimate of the deflection angle, although the $\varepsilon/R = 0.6$ angle is somewhat overpredicted, perhaps due to a slight mismatch between the measured offset and the value assigned to the simulation, and/or perhaps the absence of the downstream tubes in the platen, which are more likely to affect the $\varepsilon/R = 0.6$ jet that deflects less, and the absence of the tube stand. Nevertheless, given the complexities of these flows, the agreement with experiment is very good.

3.2 Sootblower jet flow into a generating bank

Finally, we present results of even more complex phenomena, of jet flows directed into an array of tubes representative of a typical generating bank. The corresponding experimental results were obtained by schlieren imaging of a jet penetrating into an experimental array of 10 x 4 tubes (at 1/4 scale) [15]. Figure 9 illustrates the geometry of these experiments, including a definition of the offset ε/R.

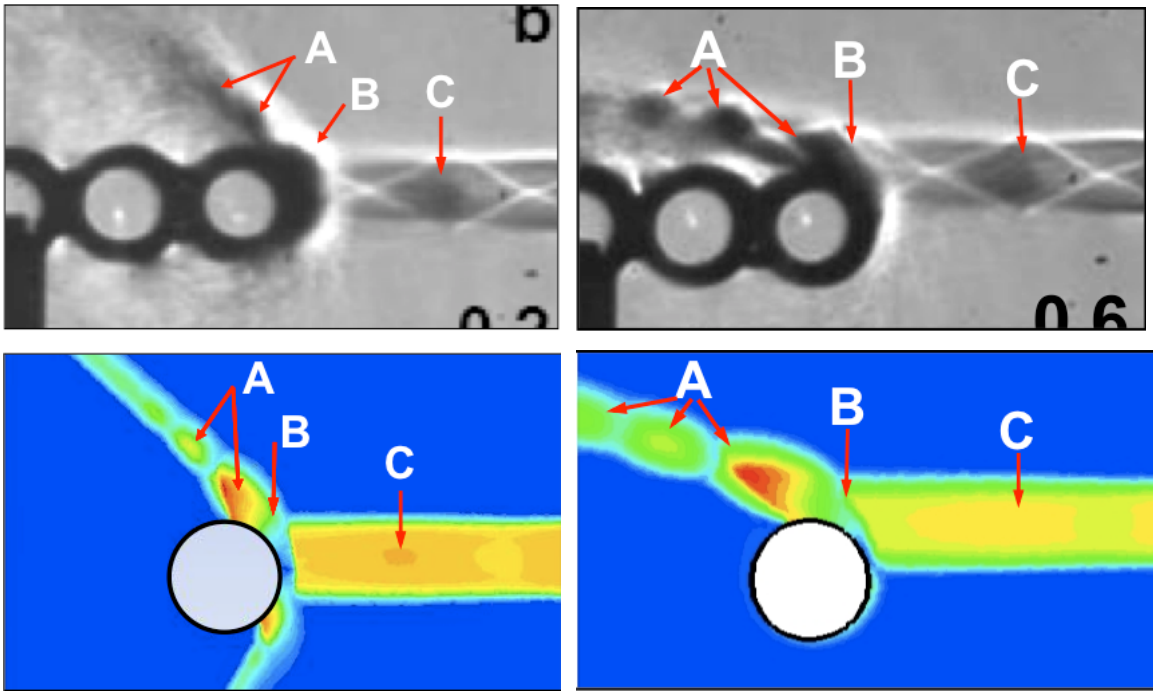

Figure 8. Schlieren images (top) of jet Mach number contours for the off-design jet of Norum and Seiner [13], and corresponding Fluent Mach number contours (bottom). Red indicates regions of highest Mach number; green of lower Mach number. Results on the left are at an offset ε/R = 0.2, and on the right at ε/R = 0.6.

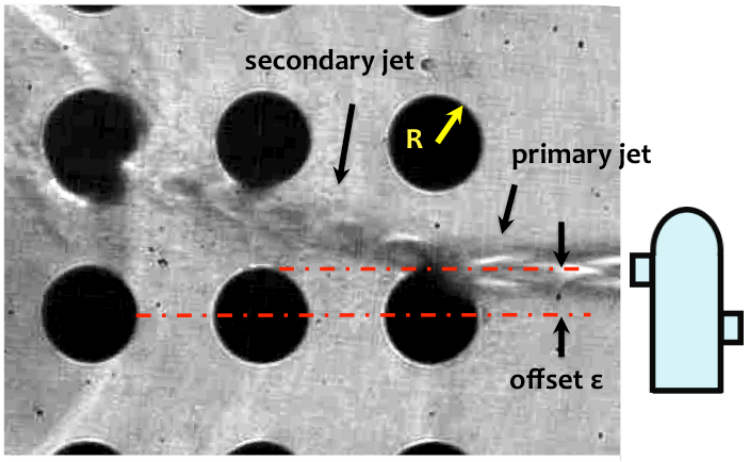

Figure 9. Geometry of a sootblower jet directed into a generating bank. The offset ε is defined as the distance between the centerline of a row of tubes and the centerline of the primary jet.

Figure 10 illustrates a set of six results at different offsets, from a head-on impingement ($\varepsilon/R = 0$) to an flow that is nearly between two rows of tubes ($\varepsilon/R = 1.33$). The Fluent predictions are surprisingly accurate, at least in terms of the large-scale measures of the flow, as evidenced by the good agreement between experimental and predicted deflection angles associated with the secondary jets, and the downstream positions at which the secondary jets impinge on interior tubes in the array. Notice too that the simulations illustrate features of the flow that are less visible in the schlieren images, including the curved flow around tubes impinged by both primary and secondary jets.

Finally, Figures 12 and 13 illustrate pressure distributions on tubes impacted by the primary and secondary jets, respectively, and Table 1 presents the corresponding maximum pressures exerted on those tubes. Figure 12 illustrates the total pressure distribution for the 90^o range illustrated in Figure 11, and together with the results of Table 1 makes clear that the maximum total pressure exerted on the first tube impacted is relatively constant (at about 1 MPa) for offsets from 0 to 0.77, and that it's only the jet at $\varepsilon/R = 1.05$ that exerts a noticeably lower pressure on that quadrant of the first tube. Figure 13 shows corresponding pressures exerted on the interior tube that interacts most closely with the secondary jet, and in this case it's clear that only the jets at $\varepsilon/R = 0.77$ and 1.05 exert an appreciable pressure on downstream tubes. Even then, the maximum pressures are only about 20% of the pressure exerted by the same jet on the first tube, a clear indication that secondary jets are much weaker, and thus much less effective at removing deposits that build up in those areas.

4 CONCLUSIONS

A CFD model has been developed to accurately predict the flow of a turbulent supersonic sootblower jet, by applying various corrections to the standard k-ε turbulence model. The model yields accurate predictions for a wide range of flow behavior, from fully-expanded jets to the much more complicated off-design jets that are characterized by multi-cell shock structures, as evidenced by many validation tests against experimental data obtained in our own lab and data available in the scientific literature. The predictions are in many cases surprisingly good, given the uncertainty associated with some of the data and the complexity of these flows, and demonstrate that the model appears well-suited to predict a wide range of sootblower jet behavior. A version of this corrected turbulence model has recently been implemented into the commercial CFD code ANSYS Fluent, and the code has been applied to examine jet flows directed at lab-scale tube geometries characteristic of superheaters and generating banks. Preliminary CFD predictions provide estimates of the pressure exerted by primary and secondary jets onto tubes in such geometries, and clearly demonstrate the efficacy of this model for future studies of sootblower jet interactions with heat exchanger geometries.

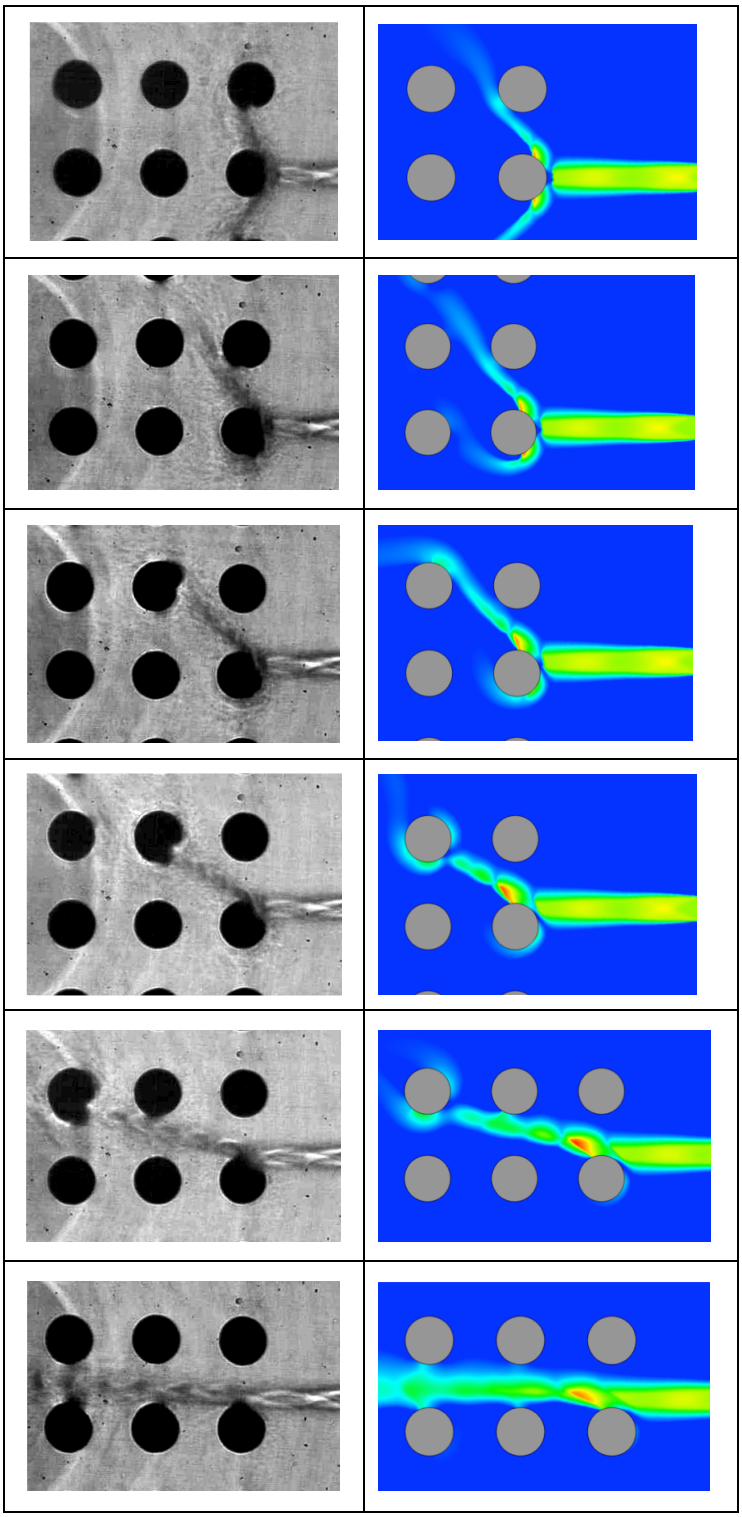

Figure 10. Schlieren images and corresponding Mach number contours of sootblower jet flow into a lab-scale generating bank geometry. From top to bottom, results correspond to ε/R = 0.00, 0.21, 0.50, 0.77, 1.05 and 1.33. Red and yellow correspond to supersonic flow; blue and green to subsonic flows.

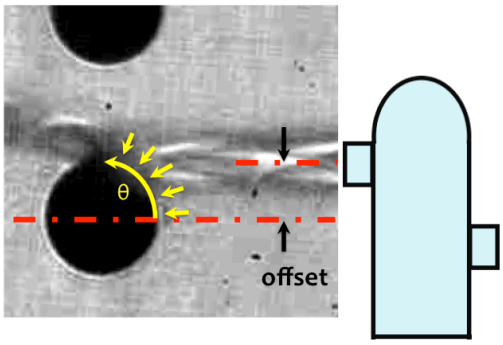

Figure 11. Definition of the angle θ in Figure 12.

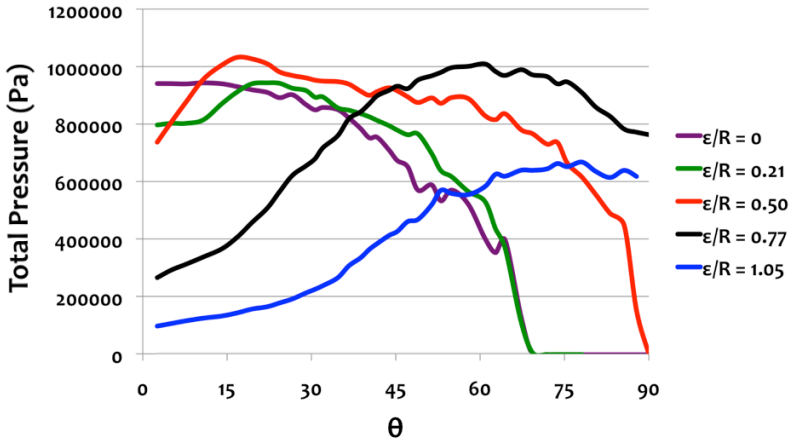

Figure 12. Total pressure distribution (as a function of θ defined in Figure 11) on the first tube impacted by a primary jet, as a function of the offset ε/R.

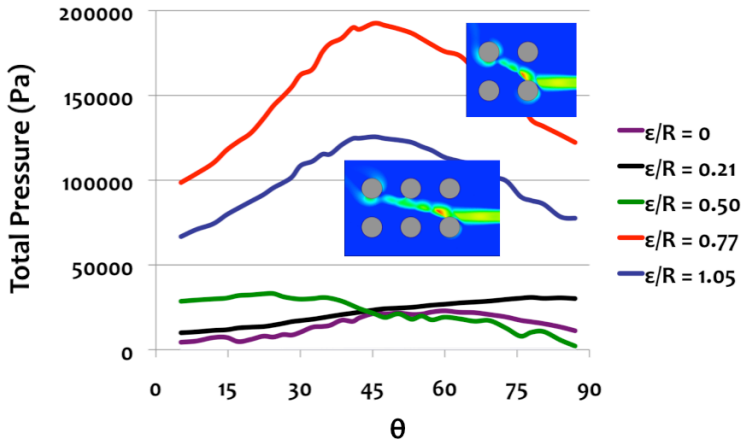

Figure 13. Total pressure distribution resulting from the interaction of a secondary jet with a downstream tube, as a function of the offset ε/R. The specific 90° range of θ varies with ε/R; for the curves corresponding to ε/R = 0.77 and 1.05, $0 < \theta < 90^{o}$ corresponds to the arc between 3 and 6 o'clock on each of these downstream tubes.

offset	max P (primary)	max P (secondary)
0	0.94 MPa	0.02 MPa
0.21	0.94	0.03
0.50	1.03	0.03
0.77	1.01	0.19
1.05	0.67	0.13

Table 1. The maximum total pressure exerted on the tube impinged by the primary jet, and on a downstream tube impinged by a secondary jet.

5 ACKNOWLEDGEMENTS

This work was conducted as part of the research program on "Increasing Energy and Chemical Recovery Efficiency in the Kraft Process", jointly supported by the Natural Sciences and Engineering Research Council of Canada (NSERC) and a consortium of the following companies: Abitibi-Bowater, Alstom Power, Andritz, Babcock & Wilcox, Boise Paper Solutions, Carter Holt Harvey, Celulose Nipo-Brasileira, Clyde-Bergemann, Domtar, DMI Peace River Pulp, Fibria, Georgia Pacific, International Paper, Irving Pulp & Paper, Metso Power, MeadWestvaco, StoraEnso Research, and Tembec. Their support is gratefully acknowledged.

6 REFERENCES

[1] A. Pophali, B. Emami, M. Bussmann, and H.N. Tran, Studies on sootblower jet dynamics and ash deposit removal in industrial boilers, *Impacts of Fuel Quality on Power Production and the Environment*," Saariselkä, Finland, August 29 - September 3, 2010.
[2] D.S. Tandra. Development and Application of a Turbulence Model for a Sootblower Jet Propagating between Recovery Boiler Superheater Platens. Ph.D. thesis, Department of Chemical Engineering and Applied Chemistry, University of Toronto, 2005.
[3] B. Emami. Numerical Simulation of Kraft Recovery Boiler Sootblower Jets. Ph.D. thesis, Department of Mechanical and Industrial Engineering, University of Toronto, 2009.
[4] D.S. Tandra, A. Kaliazine, D.E. Cormack and H.N. Tran. Numerical simulation of supersonic jet flow using a modified k-ε model. *International Journal of Computational Fluid Dynamics* 20(1): 19-27, 2006.
[5] S. Heinz, A model for the reduction of the turbulent energy redistribution by compressibility. *Physics of Fluids* 5(11): 3580-3583, 2003.
[6] P.A. Durbin, On the k-ε stagnation point anomaly. *International Journal of Heat and Fluid Flow* 17: 89-90, 1996.

[7] J. Panda and R.G. Seasholtz, Velocity and temperature measurement in supersonic free jets using spectrally resolved Rayleigh scattering. AIAA paper 99-0296, 1999.
[8] C.D. Donaldson and R.S. Snedeker. A study of free jet impingement. Part 1: Mean properties of free and impinging jets. *AIAA Journal* 45(2): 281-319, 1971.
[9] J.C. Carling and B.L. Hunt. Near wall jet of a normally impinging, uniform, axisymmetric, supersonic jet. *Journal of Fluid Mechanics* 66(1): 159-176, 1974.
[10] F. Thivet, D.D. Knight and A.A. Zheltovodov. Importance of limiting the turbulent stresses to predict 3D shock wave/boundary layer interactions. *23rd Symposium on Shock Waves*, paper 2761, 2001.
[11] K. Sinha, K. Mahesh and G.V. Candler. Modeling the effect of shock unsteadiness in shock/turbulent boundary-layer interactions. *AIAA Journal* 43(1): 586-594, 2005.
[12] B. Emami, M. Bussmann, and H.N. Tran. Application of realizability and shock unsteadiness to k- ε simulations of under-expanded axisymmetric supersonic free jets. *Journal of Fluids Engineering* 132: 041104-1-7, 2010.
[13] T.D. Norum and J.M. Seiner. Measurements of mean static pressure and far-field acoustics of shock-containing supersonic jets. NASA Technical Memorandum 84521, 1982.
[14] S. Sarkar. The pressure dilatation correlation in compressible flows. *Physics of Fluids* 4(12): 2683-2689, 1992.
[15] A. Pophali. Interaction Between a Supersonic Jet and Tubes in Kraft Recovery Boilers. Ph.D. thesis, Department of Chemical Engineering and Applied Chemistry, University of Toronto, 2011.